Available online at www.sciencedirect.com
SCIENCE DIRECT®
Journal of Solid State Chemistry 178 (2005) 3589–3594
JOURNAL OF SOLID STATE CHEMISTRY
www.elsevier.com/locate/jssc

# Independent structural and valence state transitions in the cation-ordered double perovskites $Ba_{2-x}Sr_xTbIrO_6$

Qingdi Zhou, Brendan J. Kennedy*

*Centre for Structural Biology and Chemistry, The School of Chemistry, The University of Sydney, Sydney, NSW 2006, Australia*

Received 29 June 2005; received in revised form 12 August 2005; accepted 28 August 2005

**Abstract**

Synchrotron X-ray and neutron powder diffraction were used to investigate the formation, structure and bonding in the double perovskite $Ba_{2-x}Sr_xTbIrO_6$ solid solutions. The results showed that these oxides all exhibit ordering of the Tb and Ir cations in a double perovskite-type structure. Three distinct structural types differing in symmetry and/or valence states were formed depending on the precise Ba:Sr ratio on the perovskite *A* site; $x \leqslant 0.3$ cubic ($Fm\bar{3}m$) with $Tb^{4+}$ and $Ir^{4+}$; $0.4 \leqslant x \leqslant 1.0$ cubic ($Fm\bar{3}m$) with $Tb^{3+}$ and $Ir^{5+}$ and $x \geqslant 1.2$ monoclinic ($P2_1/n$) with $Tb^{3+}$ and $Ir^{5+}$. The transitions between these appear to be first order in nature.


*Keywords:* Perovskite; Crystal structure

## 1. Introduction

The ability of transition metals to adopt multiple valence states, and to interconvert between these in response to environmental changes including lattice forces, is fundamental to much of their chemistry. As an example stable oxides are found containing Ir as +3, +4, +5 and +6 and Ir exhibits an even greater array of oxidation states in non-oxide hosts [1]. In contrast the majority of the lanthanides have only one accessible oxidation state, namely +3, due to the removal of the outermost $5d^16s^2$ electrons. Notable exceptions to this are Ce ($4f^15d^16s^2$), where the single 4*f* electron is easily removed to give $Ce^{4+}$, Pr ($4f^36s^2$), Eu ($4f^76s^2$) and Tb ($4f^96s^2$). In each case the lanthanide is found in only two oxidation states (excluding the metal). Whereas for most of the transition metal oxides valence states can be tuned by external stimuli only a relatively small number of lanthanides display this property [1–10].

Following the observation that the oxidation state of Pr was different in the two oxides $Ba_2PrRuO_6$ and $Ba_2PrIrO_6$, Wakeshima et al. [11] first demonstrated that a valence transition could be observed in the series $Ba_2PrRu_{1-x}Ir_xO_6$. Following this observation we demonstrated that the $Pr^{3+} \rightarrow Pr^{4+}$ transition could be induced by changes in either temperature or pressure [12,13]. Subsequently, we also demonstrated a similar occurrence in the related Tb oxides $Sr_2TbRu_{1-x}Ir_xO_6$ with the Ru-rich oxides having $Tb^{4+}$ and the Ir-rich oxides $Tb^{3+}$ [14]. Charge balance in both series is achieved by a concurrent valence transition in the transition metal. The role of the host lattice in controlling the valence transition remains poorly understood.

Oxides such as $Ba_2PrRuO_6$ adopt a rock-salt-ordered double perovskite-type structure, of the general form $A_2BB'O_6$. The parent $ABO_3$ perovskite structure is based on a three-dimensional network of corner sharing $BO_6$ octahedra with the larger *A*-type cation occupying the resulting 12-coordinate sites. Depending on the relative sizes of the *A* and *B* cations cooperative tilting of the $BO_6$ octahedra can occur lowering the symmetry [15]. A feature of the perovskite structure is its robustness to chemical substitutions at either the *A* or *B* sites, forming oxides such as $AB_{1-x}B'_xO_6$ [16]. Where $x = 0.5$ and the size and/or charge of the *B* and *B'* cations are sufficiently different these can order doubling the size of the unit cell [16,17]. Again tilting of the $BO_6$ and $B'O_6$ octahedra can occur giving rise to additional structural variants [18]. The oxide

*Corresponding author. Fax: +61 2 9351 3329.
*E-mail address:* kennedyb@chem.usyd.edu.au (B.J. Kennedy).

0022-4596/$ - see front matter © 2005 Elsevier Inc. All rights reserved.
doi:10.1016/j.jssc.2005.08.032

$Sr_2TbIrO_6$ is a case at point where the $TbO_6$ and $IrO_6$ octahedra order giving rise to a double perovskite structure. In addition these octahedra undergo a combination of in-phase and out-of-phase tilting due to a mismatch in the size of the Sr and *B*-type cations, with the resulting structure being monoclinic in $P2_1/n$.

The valence states of the two mixed Tb–Ir double perovskites are different, $Ba_2Tb^{4+}Ir^{4+}O_6$ and $Sr_2Tb^{3+}Ir^{5+}O_6$ [14] and this clearly presents the possibility of inducting a valence transition by doping $Ba_2TbIrO_6$ with $Sr_2TbIrO_6$, that forms oxides of the type $Ba_{2-x}Sr_xTbIrO_6$. The present paper describes the synthesis and structural characterization of a number of oxides in the series $Ba_{2-x}Sr_xTbIrO_6$. We show the presence of a first-order transition near $x = 0.35$ that is associated with a change in the valence states of the two *B*-type cations. In addition we show that these oxides display a sequence of structural phase transitions associated with the tilting of the octahedra.

## 2. Experimental

Polycrystalline samples of 16 members in the series of solid solutions $Ba_{2-x}Sr_xTbIrO_6$ were prepared by the reaction of the appropriate stoichiometric mixture of $BaCO_3$, $SrCO_3$, $Tb_4O_7$ and Ir. The reactants were intimately mixed in an agate mortar under acetone, placed in alumina crucibles and heated at temperatures of up to 1200 °C for 3 days with intermediate grindings.

The sample purity was established by powder X-ray diffraction measurements using Cu-$K\alpha$ radiation on a Shimadzu D-6000 Diffractometer. Synchrotron X-ray powder diffraction patterns were collected on the high-resolution Debye Scherrer diffractometer at beamline 20B, the Australian National Beamline Facility, at the Photon Factory, Japan [19]. The samples were finely ground and loaded into 0.3-mm glass capillaries that were rotated during the measurements. All measurements were performed under vacuum to minimize air scattering. Data were recorded using two Fuji image plates. Each image plate is $20 \times 40$ cm and covers 40° in $2\theta$. The data were collected at a wavelength of 0.80282 Å (calibrated with a NIST Si 640c standard) over the $2\theta$ range of 5–85° with step size of 0.01°.

Neutron powder diffraction data for $Ba_2TbIrO_6$ were collected at the HIFAR facility operated by the Australian Nuclear Science and Technology Organization (ANSTO) using the High Resolution Powder Diffractometer at a wavelength of 1.4928 Å [20]. The sample was held in an aluminum-capped vanadium sample holder that was rotated throughout the measurements. The diffractometer is equipped with 24 $^3$He detectors individually separated by 5°. The patterns were collected at room temperature over the $2\theta$ range 5–150° with step size of 0.05°. Structural parameters were refined by the Rietveld method using the program RIETICA [21]. A pseudo-Voigt function was used to model the peaks. The background in the synchrotron diffraction measurements was fitted by linear interpolation between regions where there were no Bragg peaks. The results of $Ba_2TbIrO_6$ obtained from the neutron diffraction data are summarized in Table 1.

Table 1
Refined structural parameters for $Ba_2TbIrO_6$ obtained using neutron powder diffraction data

| $Ba_2TbIrO_6$ space group $Fm\bar{3}m$ | | | | |
|---|---|---|---|---|
| $a$ 8.3848(2) Å | $R_p$ 5.02% | w$R_p$ 6.28% | GOF 1.68% | |
| Atom | $x$ | $y$ | $z$ | $B$ (Å$^2$) |
| Ba | $\frac{1}{4}$ | $\frac{1}{4}$ | $\frac{1}{4}$ | 0.60(3) |
| Tb | $\frac{1}{2}$ | $\frac{1}{2}$ | $\frac{1}{2}$ | 0.16(6) |
| Ir | 0 | 0 | 0 | 0.51(4) |
| O1 | 0.2350 (2) | 0 | 0 | 0.55(9) |

The numbers in parentheses are estimated standard deviations of the last significant figure. Where no standard deviation is given, the parameter was not refined.

## 3. Results and discussion

High-resolution synchrotron X-ray powder diffraction patterns have been collected for 16 members in the series $Ba_{2-x}Sr_xTbIrO_6$. An excellent fit to the pattern for $Sr_2TbIrO_6$ was obtained with a monoclinic model in $P2_1/n$. The choice of this space group was confirmed using powder neutron diffraction data, see Ref. [14] for more details. There is little obvious splitting of the main Bragg reflections indicative of monoclinic symmetry, except at high angles, Fig. 1. Similarly the superlattice reflections that are a consequence of tilting of the $MO_6$ octahedra are sufficiently weak to be effectively unobserved. The failure to observe such superlattice reflections is undoubtedly a result of the extremely strong scattering associated the heavy Tb and Ir atoms. The experimental setup easily allows observation of these types of superlattice reflections in other perovskites that lack such heavy atoms e.g. $CaMnO_3$ [22] and in the series $Ca_{1-x}Sr_xTiO_3$ [23].

Whilst the weakness of the superlattice reflections limits the precision with which the structure can be refined, see Table 2, the resolution of the diffractometer coupled with its well-defined instrumental contribution to the peak shapes [19] allows relatively precise lattice parameters to be estimated. Even with such data the high pseudo-symmetry of the metric, and the weakness of the superlattice reflections, present a challenge in this work.

Considering the synchrotron X-ray pattern for $Ba_2TbIrO_6$ we observe little if any splitting of the major Bragg reflections even at high angles, Fig. 1, and the pattern could be fitted to a cubic structure. This is not unexpected since replacing $Sr^{2+}$ with the larger $Ba^{2+}$ cation is expected to reduce the magnitude of the distortion, and in $Sr_2TbIrO_6$ such splitting were already very small. We again fail to observe well-resolved superlattice reflections diagnostic of tilting of the $MO_6$

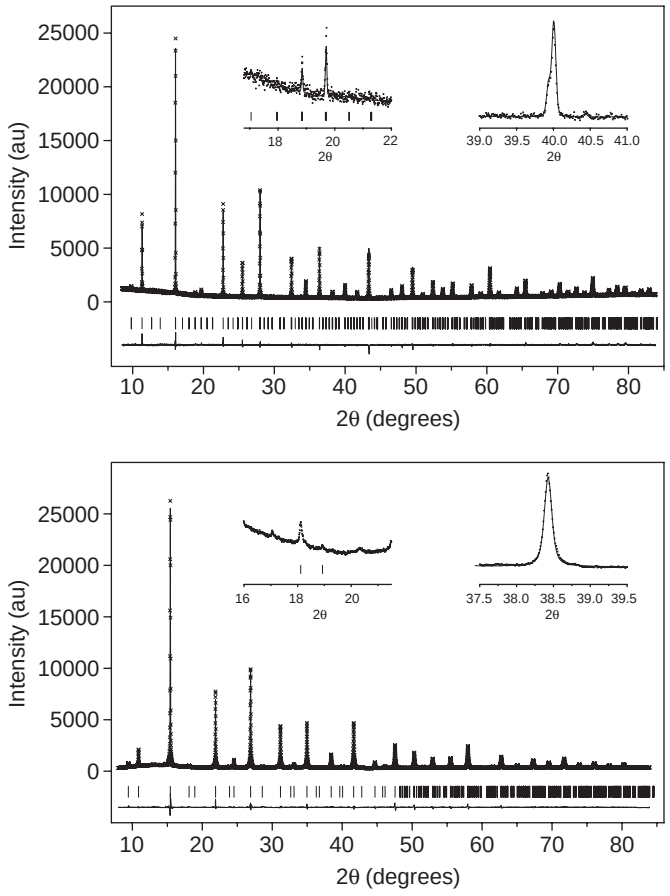


Fig. 1. Observed, calculated and difference, synchrotron X-ray diffraction profiles for $Sr_2TbIrO_6$ (top) and $Ba_2TbIrO_6$ (bottom). The two inserts highlight the weakness of the superlattice reflections indicative of tilting of the $MO_6$ octahedra near $2\theta = 18^\circ$, and the splitting of the 4 4 4-type Bragg reflection in the Sr oxide, near $2\theta = 40^\circ$.

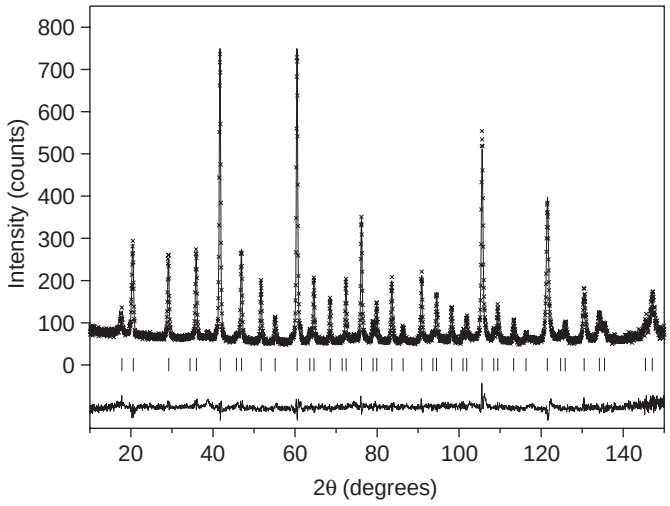


Fig. 2. Observed, calculated and difference, neutron diffraction profiles for $Ba_2TbIrO_6$.

Table 2
Refined structural parameters for $SrTbIrO_6$ obtained using synchrotron X-ray powder diffraction data

| $Sr_2TbIrO_6$ space group $P2_1/n$ | | | | |
|---|---|---|---|---|
| $a$ 5.7591(3) Å<br>$b$ 5.7506(3) Å<br>$c$ 8.1372(5) Å | $\beta$ 90.096(4) ° | $R_p$ 4.55% | w$R_p$ 5.93% | |
| Atom | $x$ | $y$ | $z$ | $B$ (Å$^2$) |
| Sr | 1.000(4) | 0.4806(7) | 0.753(2) | 0.83(4) |
| Tb | 0 | 0 | $\frac{1}{2}$ | 0.49(2) |
| Ir | 0 | 0 | 0 | 0.48(3) |
| O1 | 0.432(7) | 0.505(6) | 0.743(6) | 0.4(2) |
| O2 | 0.275(8) | 0.753(9) | 0.465(5) | 0.4(2) |
| O3 | 0.231(10) | 0.298(11) | 0.473(8) | 0.4(2) |

The displacement parameters for the three oxygen atoms were constrained to be equal.

octahedra. Resorting to neutron diffraction methods confirms that $Ba_2TbIrO_6$ is in fact cubic with only reflections indicative of cation ordering observed, Fig. 2. Refinement of the structure using powder neutron diffraction data yielded an accurate and precise structure for $Ba_2TbIrO_6$, Table 1. Refinement of the structure using the synchrotron diffraction data gave precise lattice parameters 8.3848(1) vs. 8.3848(2) Å from the neutron diffraction, but somewhat less precise values for the oxygen positional parameter (0.2307(12) vs. 0.2350(2). Despite the limitations of the method the average Tb–O 2.258(9) Å and Ir–O 1.935 (Å) distances obtained from the XRD refinement of the structure of $Ba_2TbIrO_6$ (and $Sr_2TbIrO_6$ Tb–O = 2.15(5) and Ir–O = 1.98(4) Å) are in acceptable agreement with the more accurate values obtained from the neutron diffraction data 2.222(1) and 1.970(1) Å for $Ba_2TbIrO_6$ and 2.113(1) and 2.017(1) Å in $Sr_2TbIrO_6$ (Table 3).

Having established that the two end-member oxides were not isostructural it was necessary to establish the sequence of phase transitions in these oxides. Considering the four Sr-rich oxides with $x \geqslant 1.4$, the cubic 444 reflection near $2\theta = 38^\circ$ showed clear splitting indicative of monoclinic symmetry, Fig. 3. Refinements of the structures for these four oxides in $P2_1/n$ were successful and in all cases the monoclinic angle was $\approx 90.08^\circ$. As the Sr content was decreased this splitting became smaller and for oxides with $x \leqslant 1.0$ this refection appeared as a single well-resolved peak, indicative of either tetragonal or cubic symmetry. Attempts to refine these structures in the monoclinic structure were generally unsuccessful with $\beta \approx 90.0^\circ$, physically unreasonable (negative) displacement parameters for the three independent oxygen atoms, and unacceptably large esds for the oxygen positional parameters. It was concluded that the structure of these oxides was not monoclinic.

The pattern for $x = 1.2$ $Ba_{1.2}Sr_{0.8}TbIrO_6$ was unique in this series; the 444 reflection is clearly not a singlet, Fig. 3, but the nature of the distortion is opposite to that seen in the Sr-rich oxides, in that the component at lower angle is most intense. Although the pattern could be reasonably well fitted in $P2_1/n$ this model could not reproduce the relative intensities of this reflection. As noted above an

Table 3
Refined lattice parameters, and selected measures of fit, for the series $Ba_{2-x}Sr_xTbIrO_6$ obtained using synchrotron X-ray powder diffraction data

| $X$ | Space group | $a$ (Å) | $b$ (Å) | $c$ (Å) | $\beta$ (°) | $R_p$ (%) | w$R_p$ (%) |
|---|---|---|---|---|---|---|---|
| 0 | $Fm\bar{3}m$ | 8.3848(1) | | | 90 | 3.77 | 4.27 |
| 0.1 | $Fm\bar{3}m$ | 8.3792(1) | | | 90 | 3.35 | 3.58 |
| 0.2 | $Fm\bar{3}m$ | 8.37232(9) | | | 90 | 3.23 | 3.65 |
| 0.3 | $Fm\bar{3}m$ | 8.36574(7) | | | 90 | 3.17 | 3.27 |
| 0.4 | $Fm\bar{3}m$ | 8.2700(2) | | | 90 | 4.29 | 4.52 |
| 0.5 | $Fm\bar{3}m$ | 8.2704(1) | | | 90 | 5.20 | 5.71 |
| 0.6 | $Fm\bar{3}m$ | 8.2644(1) | | | 90 | 4.66 | 5.46 |
| 0.7 | $Fm\bar{3}m$ | 8.25749(9) | | | 90 | 4.12 | 4.57 |
| 0.8 | $Fm\bar{3}m$ | 8.25088(9) | | | 90 | 3.77 | 4.51 |
| 0.9 | $Fm\bar{3}m$ | 8.240289(7) | | | 90 | 3.40 | 4.01 |
| 1 | $Fm\bar{3}m$ | 8.24310(9) | | | 90 | 3.08 | 3.75 |
| 1.2 | $P2_1/n$ | 8.2302(4) | 8.2063(2) | 8.2051(2) | 90.01(1) | 2.83 | 3.04 |
| 1.4 | $P2_1/n$ | 8.2200(1) | 8.1846(1) | 8.1828(1) | 90.08(1) | 2.57 | 2.96 |
| 1.6 | $P2_1/n$ | 8.1979(1) | 8.1675(1) | 8.1683(1) | 90.08(1) | 2.78 | 3.33 |
| 1.8 | $P2_1/n$ | 8.1733(1) | 8.1505(1) | 8.1536(1) | 90.08(1) | 2.69 | 3.23 |
| 2 | $P2_1/n$ | 8.1447(3) | 8.1327(3) | 8.1372(4) | 90.097(3) | 4.55 | 5.93 |

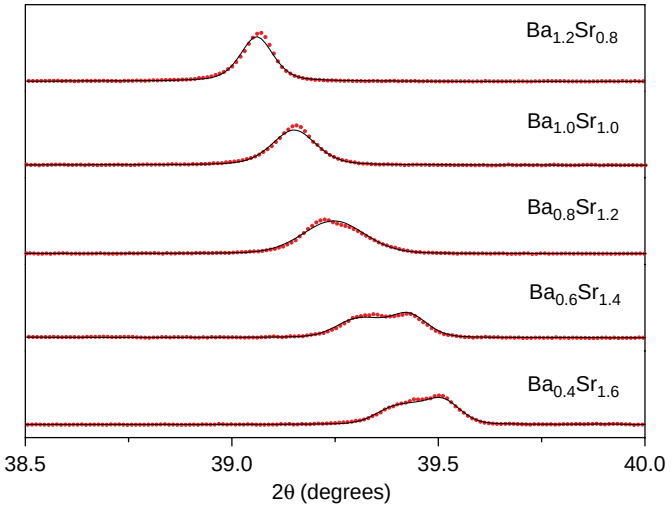


Fig. 3. Portion of the synchrotron diffraction profiles highlighting the changes in the cubic 444 reflection with composition. The solid lines are the fits to the Rietveld method in $P2_1/n$ for $Ba_{0.4}Sr_{1.6}$ and $Ba_{0.6}Sr_{1.4}$ and in $Fm\bar{3}m$ for $Ba_{1.0}Sr_{1.0}$ and $Ba_{1.2}Sr_{0.8}$. The data for $Ba_{0.8}Sr_{1.2}$ was fitted to a mixture of the two phases.

increase in the effective size of the $A$-type cation is likely to reduce the magnitude of the $MO_6$ tilts, in the extreme these become zero and a transition to a higher symmetry structure results. Considering the group theoretical analysis of Howard et al. [18], two possible tetragonal structures were identified, in $I4/m$ and $P4/mnc$. Neither of these was appropriate since they do not allow for splitting of the (cubic) 444 reflection. Since the transition from $P2_1/n$ to tetragonal or cubic must involve a first-order process, the possibility that the pattern for $Ba_{1.2}Sr_{0.8}TbIrO_6$ resulted from the coexistence of two phases was considered. A mixture of $P2_1/n$ and $I4/m$ was examined and this gave an acceptable fit although the $c/a$ ratio of the tetragonal phase was $\approx 1$ suggesting the second phase may be cubic. An equally good fit could be obtained using a two-phase $P2_1/n$–$Fm\bar{3}m$ model. These two possibilities cannot be distinguished with the available data.

Both the tetragonal and cubic models were extensively tested for the synchrotron X-ray data collected for the sample with $x = 1.0$ $Ba_{1.0}Sr_{1.0}TbIrO_6$. The pattern appears cubic and there is no resolvable splitting of any of the reflections. The use of the tetragonal model, which requires three additional variable parameters, did not result in a noticeable improvement in the quality of the fit and always gave a $c/a$ ratio of one. Consequently it was concluded that the structure of this oxide is best described in the cubic $Fm\bar{3}m$ model. It is possible that a tetragonal phase exists over a very narrow composition range.

The synchrotron patterns for the remaining eight oxides were then analyzed assuming space group $Fm\bar{3}m$. In all cases the refinements proceeded without event and resulting parameters were all physically reasonable. The composition dependence of the lattice parameters and volumes for the series $Ba_{2-x}Sr_xTbIrO_6$ is illustrated in Fig. 4. Two features should be noted from this figure. Firstly as the amount of Sr present increases ($x$ increases) the lattice parameters and volume become progressively smaller. This is in accord with the smaller ionic radii of $Sr^{2+}$ compared to $Ba^{2+}$ 1.18 vs. 1.35 Å [24]. Secondly there is a sharp discontinuity near $x = 0.35$, where the volume rapidly drops. Either side of this point the volume varies regularly with composition.

Considering the structures of the two end-members we observe the average Tb–O and Ir–O distances to be 2.113 and 2.017 Å in $Sr_2TbIrO_6$ and 2.222 and 1.970 Å, respectively, in $Ba_2TbIrO_6$. These distances are indicative of differing valence levels in the two oxides, namely $Tb^{4+}$–$Ir^{4+}$ in $Sr_2TbIrO_6$ and $Tb^{3+}$–$Ir^{5+}$ in $Ba_2TbIrO_6$. The composition dependence of the bond distances across the series $Ba_{2-x}Sr_xTbIrO_6$, illustrated in Fig. 4, shows a division of the oxides into two classes, those with long Tb–O and short Ir–O distances indicative of $Tb^{4+}$–$Ir^{4+}$

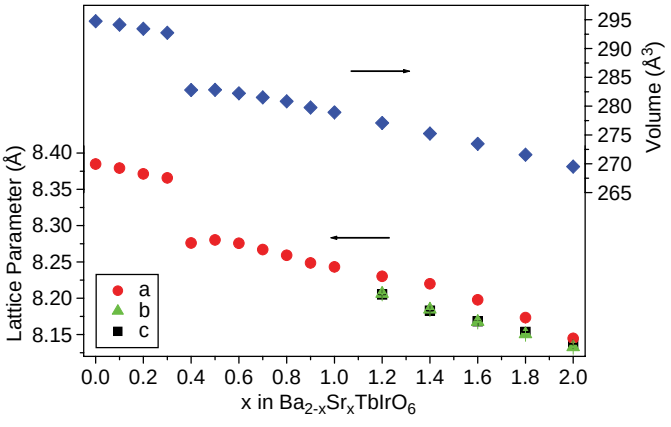


Fig. 4. Composition dependence of the lattice parameters and volumes in the series $Ba_{2-x}Sr_xTbIrO_6$. For ease of comparison the value for the $a$ and $b$-parameters in the monoclinic phase have been scaled by $2^{0.5}$.

and those with short Tb–O and long Ir–O distances indicative of $Tb^{3+}$–$Ir^{5+}$. This figure illustrates that by simply altering the size of the *A*-type cation it is possible to induce a valence transition in these oxides (Fig. 5).

The $P2_1/n$ monoclinic structure arises from the combination of cation ordering and tilting of the octahedra, the latter being described in the notation of Glazer [28] as $a^-a^-c^+$; that is, out-of-phase tilting occurs about the $[110]_p$ pseudocubic axes and in-phase tilting occurs about the $[001]_p$ axis. In the tetragonal $I4/m$ model, only out-of-phase tilting about the $[001]_p$ axis is present, $a^0a^0c^-$, whereas the cubic $Fm\bar{3}m$ structure has no tilts ($a^0a^0a^0$). Increasing the size of the *A*-type cation will reduce the magnitude of the tilts altering the M–O–M angles. Ultimately the tilts will become zero when the relative size of the type of cations is optimized.

There is no evidence from the diffraction studies for any ordering of the *A*-type cations. Give the random distribution of the the Ba and Sr cations in the solid solutions $Ba_{2-x}Sr_xTbIrO_6$ it is clear that there is a critical size for the *A*-site cation needed to stabilize each oxidation state. This is very different to the behavior previously observed in the related $Ba_2PrRu_{1-x}IrO_6$ and $Sr_2TbRu_{1-x}Ir_xO_6$ systems where the number of *d*-electrons alters across the transition. The vast literature on perovskites demonstrates that as the effective size of the *A*-type cation increases (see for example the recent book by Mitchell [16], in this case as the Ba content increases, the magnitude of the $MO_6$ octahedral tilting decreases. However, the symmetry of the oxides immediately above and below the valence transition is the same and clearly the transition is not influenced by a change in the $MO_6$ tilting. Changes in the M–O distance and M–O–M bond angles can alter the orbital overlap. Just as subtle changes in orbital overlap can induce metal-to-non-metal transitions in perovskites (e.g. $LnNiO_3$) [25,26]

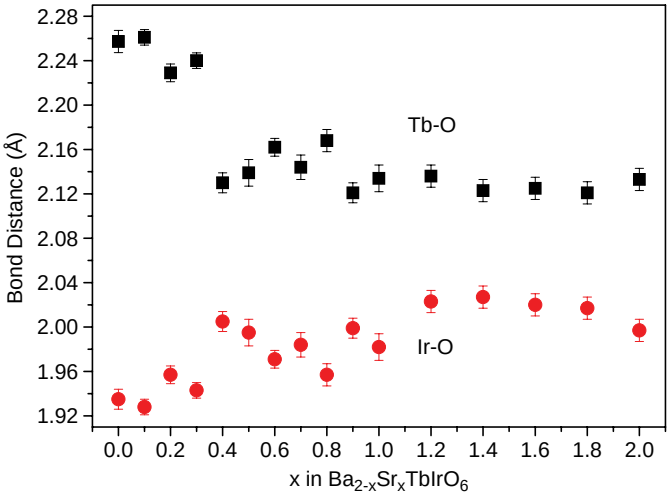


Fig. 5. Composition dependence of the average Tb–O and Ir–O bond distances in the series $Ba_{2-x}Sr_xTbIrO_6$. The large drop in the Tb–O distance near $x = 0.4$ is consistent with an increase in the Tb valence state from +3 to + 4. Likewise the decrease in the Ir–O distance corresponds to decease in valence state from +5 to +4.

and in other oxides with structures based on corner sharing $MO_6$ octahedra including pyrochlores [27] and rutiles, it is apparent from this work that changes in overlap can induce valence transitions, even where the bond angles remain the same. The best indication for a change in the local bonding network comes from the bond valence sum calculations. The effective BVS for the A-type cations in the Ba rich ($Tb^{3+}$–$Ir^{5+}$) oxides is 1.9 and this increases to 2.1 in the $Tb^{4+}$–$Ir^{4+}$ oxides. Whilist neither of these values are unusual the change is suggestive that electronic effects may be important.

The cause of the volume discontinuity at the valence transition in these types of double perovskites has been discussed in some detail previously [11–14]. Simply put the reduction in the ionic radii [24] associated with the $Tb^{3+}$–$Tb^{4+}$ transition (0.923 vs. 0.76 Å) is much greater than the increase due to the $Ir^{5+}$–$Ir^{4+}$ transition (0.57 vs. 0.625 Å). Hence, the volume of the $TbO_6$ octahedra decreases by more than the volume of the $IrO_6$ octahedra increases resulting in an overall reduction in cell volume. The observation that this discontinuity occurs at a well-defined composition (near $x = 0.35$) shows this transition to be first order.

In conclusion we have observed two types of transitions in the series $Ba_{2-x}Sr_xTbIrO_6$ upon altering the Ba:Sr ratio, the first near $x = 0.35$ is associated with a Tb–Ir valence transition that is not associated with any change in space group symmetry and the second near $x = 1.2$ is associated with a symmetry change as a consequence of a zone boundary instability. This represents a significant advance on our studies of valence transitions in these types of oxides, in that in all other systems studied to date it has been necessary to dope into the perovskite-*B* sites, consequently changing the total number of valence electrons. In the present series the number of valence electrons remains constant and the transition is driven by steric factors, most probably changes in the M–O–M overlap. Although the transition from $P2_1/n$ to $Fm3m$ results in a change in the effective coordination number of the *A*-type cation from 9 to 12-coordinate this does not drive the transition. It will be interesting to establish the temperature and pressure dependence of these two transitions. Like wise detailed band structure calculations would be illuminating.

## Acknowledgments

BJK thanks the Australian Research Council for support for his work on perovskites. The work performed at the Australian National Beamline Facility was supported by the Australian Synchrotron Research Program, which is funded by the Commonwealth of Australia under the Major National Research Facilities program. The Australian Institute of Nuclear Science and Engineering supported the neutron diffraction experiments. The assistance of Dr. Margaret Elcombe with the collection of the Neutron Diffraction data is gratefully acknowledged.

## References


[1] S.A. Cotton, Chemistry of Precious Metals, Springer, Berlin, 1997.
[2] P.A. Cox, Transition Metal Oxides: an Introduction to their Electronic Structure and Properties, Clarendon Press, Oxford, 1992.
[3] J.M. Lawrence, P.S. Riseborough, R.D. Parks, Rep. Prog. Phys. 44 (1981) 1.
[4] A. Jayaraman, V. Narayanamurti, E. Bucher, R.G. Maines, Phys. Rev. Lett. 25 (1970) 1430.
[5] J.L. Sarrao, A.P. Ramirez, T.W. Darling, F. Freibert, A. Migliori, C.D. Immer, Z. Fisk, Y. Uwatoko, Phys. Rev. B 58 (1998) 409.
[6] Y. Doi, Y. Hinatsu, K. Oikawa, Y. Shimojo, Y. Morii, J. Mater. Chem. 10 (2000) 1731.
[7] A. Jayaraman, G.A. Kourouklis, L.G. Van Uitert, Phys. Rev. B 36 (1987) 8547.
[8] P.M. Woodward, D.E. Cox, E. Moshopoulou, A.W. Sleight, S. Morimoto, Phys. Rev. B 62 (2000) 844.
[9] Y. Doi, Y. Hinatsu, K. Oikawa, Y. Shimojo, Y. Morii, J. Mater. Chem. 10 (2000) 1731.
[10] M. Wakeshima, D. Harada, Y. Hinatsu, J. Mater. Chem. 10 (2000) 419.
[11] M. Wakeshima, Y. Izumiyama, Y. Doi, Y. Hinatsu, Solid State Commun. 120 (2001) 273.
[12] L. Li, B.J. Kennedy, J. Solid State Chem. 177 (2004) 3290.
[13] B.J. Kennedy, L. Li, Y. Lee, T. Vogt, J. Phys. Condens. Matter 16 (2004) 3295.
[14] Q. Zhou, B.J. Kennedy, K.S. Wallwork, M.M. Elcombe, Y. Lee, T. Vogt, J Solid State Chem. 178 (2005) 2282.
[15] C.J. Howard, H.T. Stokes, Acta Crystallogr., Sect B: Struct. Sci. 54 (1998) 782.
[16] R.H. Mitchell, Perovskites: Modern and Ancient, Almaz Press, Ontario, Canada, 2002.
[17] M.T. Anderson, K.B. Greenwood, G.A. Taylor, K.R. Poeppelmeir, Prog. Solid St. Chem. 22 (1993) 197.
[18] C.J. Howard, B.J. Kennedy, P.M. Woodward, Acta Crystallogr., Sect B: Struct. Sci. B 59 (2003) 463.
[19] T.M. Sabine, B.J. Kennedy, R.F. Garrett, G.J. Foran, D.J. Cookson, J. Appl. Crystallogr. 28 (1995) 513.
[20] C.J. Howard, C.J. Ball, R.L. Davis, M.M. Elcombe, Aust. J. Phys. 36 (1983) 507.
[21] C.J. Howard, B.A. Hunter, A Computer Program for Rietveld Analysis of X-ray and Neutron Powder Diffraction Patterns, Lucas Heights Research Laboratories, 1998, pp. 1–27.
[22] Q. Zhou, B.J. Kennedy, J. Phys. Chem. Solids, submitted for publication.
[23] C.J. Ball, B.D. Begg, D.J. Cookson, G.J. Thorogood, E.R. Vance, J. Solid State Chem. 139 (1998) 238.
[24] R.D. Shannon, Acta Crystallogr. A 32 (1976) 751.
[25] J.A. Alonso, M.J. Martinez-Lope, M.T. Casais, J.L. Garcia-Munoz, M.T. Fernandez-Diaz, M.A. Aranda, Phys. Rev. B 64 (2001) 094102.
[26] T. Saito, M. Azuma, E. Nishibori, M. Takata, M. Sakata, N. Nakayama, T. Arima, T. Kimura, C. Urano, M. Takano, Physica B—Condens. Matter 329 (2003) 866.
[27] L. Li, B.J. Kennedy, Chem. Mater. 15 (2003) 4060.
[28] A.M. Glazer, Acta Crystallogr., Sect B: Struct. Crystallogr. Cryst. Chem. B 28 (1972) 3384.